NMR IN BIOMEDICINE
NMR Biomed. 2007; **20**: 291–303
Published online in Wiley InterScience
(www.interscience.wiley.com) DOI:10.1002/nbm.1142

Review Article

MR technology for biological studies in mice

Brian J. Nieman,[1,2] Jonathan Bishop,[1] Jun Dazai,[1†] Nicholas A. Bock,[3] Jason P. Lerch,[1] Akiva Feintuch,[1] X. Josette Chen,[1,2] John G. Sled[1,2] and R. Mark Henkelman[1,2*]

[1]Mouse Imaging Centre, Hospital for Sick Children, Toronto, Canada
[2]Department of Medical Biophysics, University of Toronto, Toronto, Canada
[3]Cerebral Microcirculation Unit/ Laboratory of Functional and Molecular Imaging, NINDS/NIH, Bethesda, MD, USA

Received 5 June 2006; Revised 30 November 2006; Accepted 30 November 2006

ABSTRACT: Mouse models are crucial for the study of genetic factors and processes that influence human disease. In addition to tools for measuring genetic expression and establishing genotype, tools to accurately and comparatively assess mouse phenotype are essential in order to characterize pathology and make comparisons with human disease. MRI provides a powerful means of evaluating various anatomical and functional changes and hence is growing in popularity as a phenotypic readout for biomedical research studies. To accommodate the large numbers of mice needed in most biological studies, mouse MRI must offer high-throughput image acquisition and efficient image analysis. This article reviews the technology of multiple-mouse MRI, a method that images multiple mice or specimens simultaneously as a means of enabling high-throughput studies. Aspects of image acquisition and computational analysis in multiple-mouse studies are also described. Copyright © 2007 John Wiley & Sons, Ltd.

KEYWORDS: mouse imaging; multiple-mouse MRI; mouse phenotype

INTRODUCTION

An improved understanding of genetic factors directing the complex processes of normal and disease development will open up new avenues for the treatment of human disease. However, with ~25 000 genes (1) and a high level of heterogeneity (2–4) in the human genome, the task of identifying the precise role of each gene and the complex interplay between them is overwhelming. As a result, it is tremendously beneficial to study other closely related mammals, in which genetic and experimental conditions can be better defined and even controlled. In no other mammal is this more true than the mouse. With the availability of genetically homogeneous mouse strains and the ability to manipulate the mouse genome, the mouse is an optimal choice for biomedical research.

In mouse studies of disease, concise yet thorough evaluation of both genotype and phenotype are necessary. Serial evaluation of individual genes or traits is impractical. Consequently, strategies for simplifying analyses or improving efficiency are being developed. For instance, although genotype descriptions can be simplified by experimentation with only a single gene at a time, many conditions lack candidate genes of interest or appear to have only incomplete lists of implicated genes. Alternative methods that accommodate a number of genes in parallel are desirable. To this end, technologies for efficient and indiscriminate genetic alteration and detection have been developed. As examples, chemical mutagenesis permits rapid genome-wide alteration of genes (5,6) and DNA microarrays simultaneously probe the expression levels of thousands of genes (7,8). In the same fashion, the evaluation of mouse phenotype must be streamlined. As assessment of isolated phenotypes is not generally applicable, technology permitting rapid and comprehensive assessment is necessary. The systematic, phenotype-driven evaluation of disease status has important applications for routine screening of novel mutations and for more detailed studies of particular disease models. A number of methods are being developed for this purpose. Noteworthy among these are several medical imaging techniques that are routinely used for diagnosis in the human population.

In particular, MRI is known for excellent soft tissue visualization throughout the body. Simple T_1-weighted and T_2-weighted images, providing anatomical and

**Correspondence to:* R. M. Henkelman, Mouse Imaging Centre, Hospital for Sick Children, 555 University Avenue, Toronto, Ontario, Canada M5G 1X8.
E-mail: mhenkel@phenogenomics.ca
†Disclosers: J. Dazai is founder of Dazai Research Instruments, manufacturer of the mouse sled described in this article.
Contract/grant sponsor: Canada Foundation for Innovation/Ontario Innovation Trust, Ontario Research and Development Challenge Fund, and the National Institutes of Health.

Abbreviations used: ECG, electrocardiography; RF, radiofrequency; SNR, signal-to-noise ratio; FOV, field-of-view; MMMRI, multiple-mouse MRI.

morphological characterization, remain the backbone of most clinical diagnostic scans. Increasingly, however, various means of functional characterization have become available, including measurements of blood flow, dynamic tissue motion, hemodynamics associated with neuronal function and other tissue properties. In addition, there is a growing new industry focused on molecular-specific imaging. These MRI techniques are well suited for development and implementation at the scale of the mouse.

Although mouse MRI shares similarities with clinical MRI, it is important to also recognize important differences. First of all, at resolutions permitting comparable organ coverage, scan duration is generally longer in mice than in humans. The increase in imaging time – in combination with dedicated mouse radio-frequency (RF) coils and high field MR systems – is necessary for sufficient signal-to-noise ratio (SNR) in mouse imaging studies, which are more signal-limited than human studies. Second, the aim in typical mouse studies is characterization of a population rather than diagnosis of an individual. Biomedical research studies always include a number of mice in order to assess phenotype variability and penetrance as well as increase statistical power. This switch to multiple subject datasets motivates a philosophical shift at the scanner during image acquisition, with a focus on animal throughput (as highlighted recently by McConville *et al*. (9)). Furthermore, a third and related difference is encountered during image analysis of multiple subject datasets. Two or more different groups of mice must be collectively compared with one another, in contrast with clinical diagnosis, which is based on the detailed consideration of one or more images from a single individual. Such population-based analyses have already been pioneered in select research studies evaluating data from large groups of human images (10–17), and must become an integral part of mouse imaging studies. These important differences necessitate modification of traditional clinical MRI technology for use in the mouse.

This article reviews innovations developed at the Mouse Imaging Centre in Toronto for mouse MRI. These innovations address the throughput requirements of image acquisition and analysis encountered over the course of a typical mouse study, making MRI more useful for various biomedical studies. The first section describes multiple-mouse MRI (MMMRI), a technique that greatly increases mouse throughput by parallelization of the imaging process. Subsequent sections describe *in vivo* and fixed-specimen MMMRI implementations. Analysis of multiple-mouse image datasets is the topic of the final section, where an example *in vivo* study is also presented. We have placed an emphasis in this paper on the technical aspects of high-throughput imaging; a review of mouse phenotyping by MRI is provided elsewhere in this issue.

HIGH-THROUGHPUT IMAGING FOR MOUSE STUDIES: MMMRI

Theory

Various techniques for increasing image throughput in mouse studies can be envisaged. Rapidly imaging mice in a serial fashion inevitably sacrifices image quality; as mouse imaging is already SNR-limited, alternative means of increasing throughput are preferred. Parallelization of the imaging process, so that multiple mice can be imaged simultaneously is an effective way of reducing scan time on a per mouse basis without sacrificing MR protocol flexibility. This is the motivation behind MMMRI.

Several different hardware configurations for imaging mice in parallel are possible. These were examined by Bock *et al*. (18). Many of the possible configurations have since been demonstrated, and include the simple case of a single RF coil and gradient set with multiple close-packed mice (19,20) as well as the more complex case of individual RF and gradient coils for each of multiple mice (21). A recent review from our group (22) includes a more extensive discussion and comparison of these alternatives. Provision of an individually shielded, single-mouse RF coil for each of multiple mice in a common gradient set is one of the most efficient arrangements. In this configuration, the improved sensitivity of small volume RF coils for each mouse is maintained, and the fraction of the homogeneous magnetic field occupied by additional MMMRI hardware is kept at a minimum. A picture of this system as implemented at our laboratory is provided in Fig. 1. As many as 19 RF coils set in a close-packed array are placed within a full-bore gradient. Although RF transmission and reception is independent for each coil, they are timed coincidently so that spatial encoding is achieved with a single set of gradient pulses.

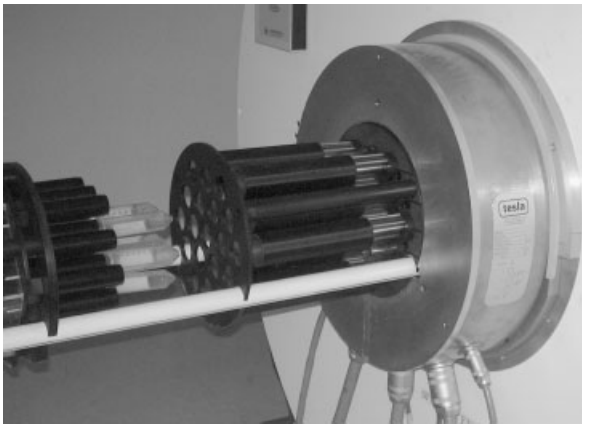

Figure 1. MMMRI hardware for a dedicated 7 T system. An array of 16 RF coils is shown partly removed from the bore of a common gradient set, which provides spatial encoding for mice in all coils. A loading array set on the rails at the left holds centrifuge tubes, in which mice reside during the imaging session.

DOI: 10.1002/nbm

Throughput increase is achieved by acquiring mouse images from all coils simultaneously. Nevertheless, image prescription proceeds as if only a single mouse were present. A field-of-view (FOV) is set to cover a single mouse in the center RF coil, and the desired imaging parameters are selected. Data acquisition and reconstruction for this coil then proceed exactly as if only a single mouse were imaged. However, signal is also acquired from the additional coils and their respective mice. As these coils are located at positions corresponding to frequencies beyond the Nyquist limit of the single-mouse FOV, data are aliased in these images and may appear wrapped across image edges as opposed to being properly centered. The aliasing is described precisely by the mouse position in the bore, such that coils displaced by a non-integer multiple of the FOV produce images in which the mouse appears off-center for a Cartesian acquisition. A simple phase correction of the acquired data based on coil position can be used as a routine part of the reconstruction to correct aliased images. Alternatively, Cartesian data acquisitions can be empirically ''cut-and-pasted'' together after image reconstruction by unwrapping image data about an appropriately selected origin. These changes represent only minor modifications to the reconstruction procedure. Similarly, potential distortions due to gradient nonlinearity at the periphery of the coil array can be mapped and then corrected during image reconstruction, analogous to practices standard on clinical MRI systems (23). Hence, MMMRI permits multiple channels of data acquisition during the acquisition of a single-mouse image without time costs or sacrifices in image quality.

MMMRI is sufficiently flexible that nearly all MRI sequences can be modified for use in high-throughput studies; individual RF events in a pulse sequence simply need to be parallelized. Some limitations apply to two-dimensional MMMRI sequences because of the common gradient; slices in different mice must be strictly parallel. This may provide satisfactory results for some studies (as, for instance, in the cancer study by Bock *et al.* (24)), but the possibility of postural differences between mice introduces a distinct preference for three-dimensional isotropic imaging. In any case, the preference for three-dimensional imaging seems to be a general trend even for single-mouse imaging systems; this trend is in part due to post-acquisition analysis methods for several images, which are improved by isotropic data independent of whether images were collected in series or in parallel. There is even a growing use of isotropic three-dimensional imaging with phased array and sensitivity encoding in human imaging because it allows easier acquisition and more flexible retrospective analysis (25). Thus, in general, sequence design is not hampered by MMMRI methods.

Implementation of MMMRI was recently validated using a dedicated 7 T scanner (26). Quality of individual images was compared carefully to ensure equivalency. Parameters that might differentially affect MMMRI images, such as gradient linearity, B_0 field homogeneity and RF coil isolation, were measured, corrected where necessary, and determined to be sufficiently homogeneous across the bore so as to permit quantitative comparison of images in different coil positions. Simultaneous acquisition of seven *in vivo* mouse images and 16 fixed-mouse images was demonstrated. Image quality in multiple-mouse images has been shown to be equivalent to a single-mouse image acquired by the same protocol. An example MMMRI dataset is provided in Fig. 2, where six fixed mice were imaged simultaneously.

Volume coil hardware

The RF receive coil is the single largest factor influencing SNR in MRI experiments, and hence coil selection is critical for mouse imaging experiments. Birdcage coils offer a convenient geometry because they may be placed coaxially with the bore of the magnet for easy loading and unloading of mice. To optimize SNR performance, the coil diameter should be chosen as small as possible while matching the homogeneous RF region to the size of a mouse. A many-rung birdcage coil design is advantageous, as the homogeneous region fills a larger fraction of the coil volume. Our system uses the Millipede^{TM} coil (27) (Varian Inc., Palo Alto, CA, USA), which includes hundreds of rungs and extends the homogeneous region of the coil to fill most of the interior coil diameter. In addition to coil diameter, coil length must be matched to the region of interest. We have two millipede coil arrays, with 40 and 110 mm longitudinal FOVs. The shorter coil set, appropriate for imaging in the brain, heart, lung or other isolated organs, was measured to have a twofold higher SNR than the longer coil set, which is designed for whole-body imaging applications.

In MMMRI, it is also important to shield coils from one another to avoid ghosting between imaging channels. A cylindrical RF shield placed coaxially with each RF coil is the simplest geometry. Although alternative shield shapes have been described (18), a cylindrical shape has the advantage of flexibility in packing geometry and ease of construction. With proper shielding, nearly complete isolation between channels can be achieved so that images are ghost free, in spite of the close proximity of other samples.

Mouse handling hardware

Although there is little or no time cost associated with the prescription and acquisition of MMMRI images, mouse preparation still requires individual handling. To minimize the effect on multiple-mouse imaging efficiency, we have built custom hardware for the processes of mouse

DOI: 10.1002/nbm

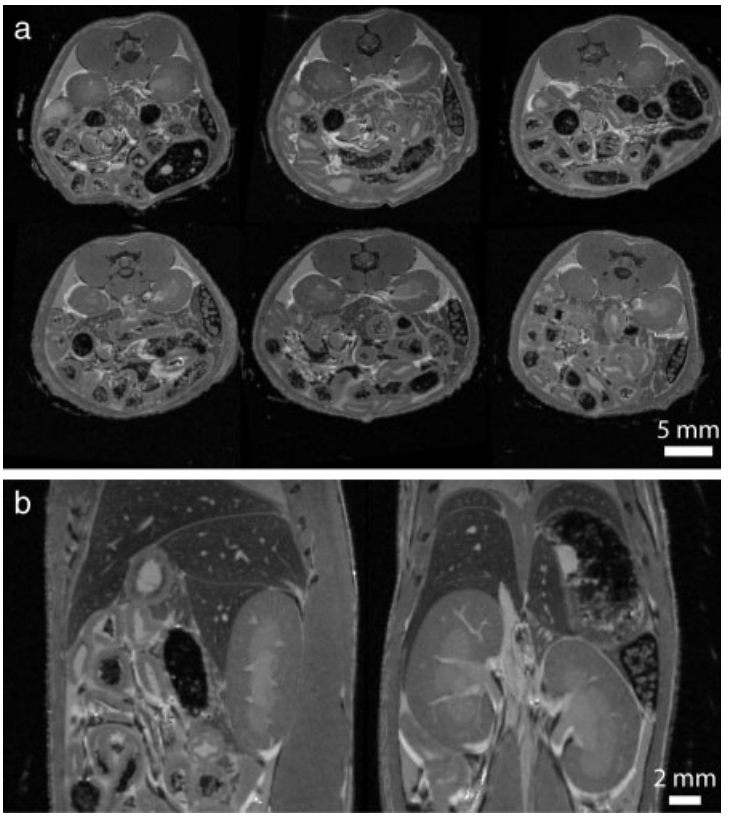

Figure 2. MMMRI data acquisition in fixed mice. Images of the abdomen of six fixed mice were acquired simultaneously in a single overnight scan session. In (a), an axial slice through each of the datasets is shown. In (b), orthogonal sagittal and horizontal slices are shown from an individual mouse, indicating the three-dimensional nature of the data acquisition in each of the six images. The images were acquired with a three-dimensional spin-echo pulse sequence ($TR/TE = 600/14$ ms; matrix $= 300 \times 270 \times 270$, $30 \times 27 \times 27$ mm FOV; 12 h 10 min total scan time).

preparation and positioning within the coil (28). A recent version of this hardware is indicated in Fig. 3. Mice are anesthetized simultaneously in a large induction chamber with iris ports which allow access for mouse handling. Within the chamber, mice are each prepared individually and then placed in centrifuge tubes that mount on a loading array. The loading array slides along rails into the bore and positions each centrifuge tube snugly against

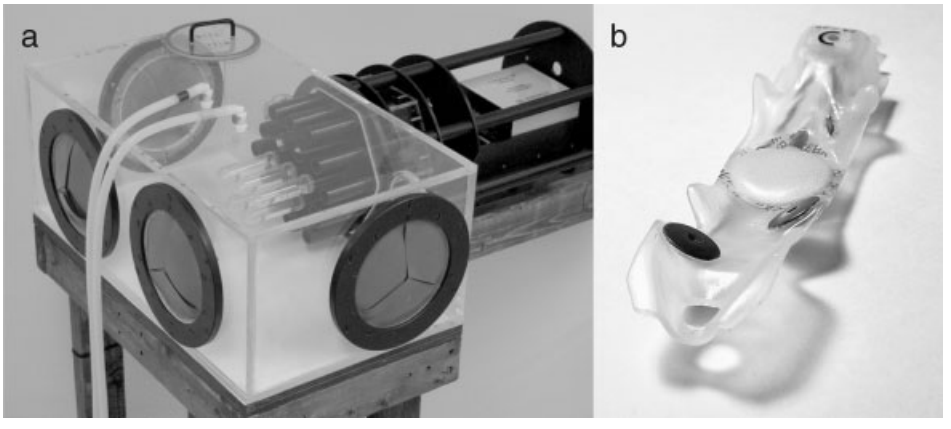

Figure 3. MMMRI hardware for mouse preparation. In (a), a mouse loading array, also shown on the left in Fig. 1, is shown docked into the induction chamber, where mice can be prepared under anesthesia before imaging. As part of the preparation, mice are placed on the mouse sled shown in (b), which incorporates devices for monitoring heart rate, respiratory events and temperature. Sled photo courtesy of Dazai Research Instruments.

DOI: 10.1002/nbm

nose cones which deliver gaseous anesthetic to each mouse. Loading of seven mice with this system can be achieved in approximately 24 min. This corresponds to only 3.5 min per mouse, an average time significantly faster than can be achieved by serially preparing and loading individual mice.

Physiological monitoring of mice during *in vivo* imaging must be parallelized as well. Obtaining high-quality physiological signals becomes particularly critical in motion-gated MR sequences. As setting up physiological monitoring can be time consuming, mouse sleds have been designed that incorporate non-invasive electrocardiography (ECG), temperature and pneumatic respiratory probes as shown in Fig. 3b (Dazai Research Instruments, Toronto, Canada). Physiological monitoring can thus be achieved by simple placement of the mouse on the sled (after chemical hair removal at ECG sites on the mouse chest). The sled is designed to slide into the centrifuge tube with the mouse and includes electronic leads to transmit physiological data from the sleds out of the MR scanner. Physiological signals can then be displayed, stored for later processing, or used for gating as desired with appropriate monitoring equipment (built for us by SA Instruments, Inc., Stony Brook, NY, USA).

IN VIVO IMAGING WITH MMMRI

Mouse imaging requirements

The *in vivo* evaluation of disease in the mouse is the most attractive benefit of mouse MRI in biomedical research. Ideally, all of the sequences used in human MRI, including various anatomical, diffusion, functional, cine, quantitative and other specialized imaging methods, also need to be available for live mouse imaging. This not only permits direct comparison of human disease manifestations with mouse models, but also greatly expands the measurements currently available for mouse phenotyping. The implementation of many sophisticated imaging sequences has already been reported in the mouse, including diffusion-weighted and diffusion tensor imaging (29–32), dynamic cardiac imaging (33–38), magnetization transfer imaging (39–41), and functional MRI (42–47) among others. The successful application of these sequences suggests that, for the most part, clinical imaging experience can be translated to mouse applications with few limitations.

In addition to analogs of human studies, several opportunities are uniquely available to mouse imaging. The mouse provides an excellent model for the development of novel contrast agents and the design of molecular imaging methods (48,49). For example, transgenic mouse models of Alzheimer's disease have been used for research into amyloid-specific contrast agents (50,51). Alternatively, some contrast agents can be used in mice, but will remain unavailable in human studies because of toxicity. Manganese is a pertinent example that highlights active transport of calcium in functioning neurons (52–56). Another example is the use of modified genetic expression that generates contrast on MR images and continues to be expressed by all progeny cells (57,58). These opportunities in mice, although not necessarily intended for translation to human clinical applications, have important implications for treatment and diagnosis of disease and consequently motivate continued development of *in vivo* mouse MRI. Each of these mouse imaging sequences must also be available for high-throughput MMMRI.

Significant efforts to eliminate motion artifacts are required for *in vivo* mouse MRI, as in clinical MRI. Physiological motions in the mouse are much faster than in the human (600 bpm heart rate compared with 70 bpm in the human). In some cases, such as neuroimaging, motion artifacts can be eliminated with simple restraints. In general, however, artifact-free images require more sophisticated methods. In the human clinical experience, the gold standard for eliminating physiological motion artifacts is prospective cardiac and respiratory gating often including breath-holding. These methods have been successfully implemented in the mouse as well (59) (although obviously without breath-holding), but are clearly inappropriate for multiple-mouse acquisitions. An alternative gating strategy amenable to MMMRI is required.

Retrospective gating for multiple-mouse cardiac MRI

As physiological motion such as heart beats and respiratory events do not occur simultaneously in multiple animals, a gating technique that accommodates asynchronous motion is required for MMMRI. Various forms of retrospective gating developed originally for human cardiac imaging provide candidate methods (60,61). In principle, any method that permits the parallelization of gating signal acquisition and does not rely on real time adaptation can be implemented in multiple mice. Techniques dependent on peripheral physiological monitoring devices such as ECG and respiratory pillows are MMMRI-compatible, as physiological data can be collected and stored from each mouse independently. Similarly, self-gating methods or navigator echo techniques that detect motion directly from MR data are appropriate. In either case, reconstructions in a motion-gated MMMRI acquisition are performed independently with the processing, sorting and/or discarding of data tailored for each mouse.

Retrospective gating for cardiac imaging has been recently demonstrated in mice (62). In a single mouse, retrospectively gated images were found to be of comparable quality to prospectively gated images. Extension to MMMRI in three mice demonstrated the

DOI: 10.1002/nbm

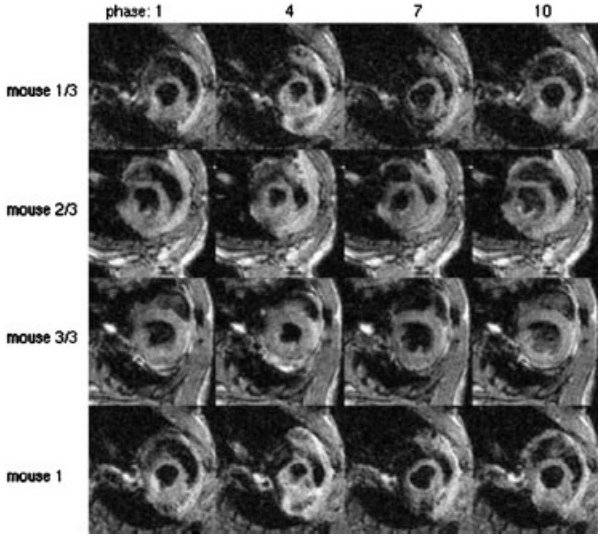

Figure 4. MMMRI cardiac acquisition with retrospective gating. An axial slice through the heart taken from isotropic rectilinearly acquired datasets is shown in three mice imaged simultaneously with MMMRI. Retrospective gating was used, and 10 phases of the heart cycle were generated (four are shown). The bottom row shows mouse 1 imaged in a single acquisition. Reprinted from reference (62) with permission from John Wiley & Sons, Inc.

acquisition of three separate cardiac cine images with 10 phases per heart cycle and 200 μm in-plane resolution. Cardiac images in multiple mice were of equivalent quality to identical scans run in a single mouse (Fig. 4), demonstrating the practicality of gated MMMRI.

In vivo whole-body imaging

With the success of gating in single and multiple mice, it is interesting to consider the prospect of whole-body imaging in mice. In the human population, whole-body imaging has been proposed as a means of screening cancer patients for evidence of metastases or even healthy individuals for early detection of pathology. It can be achieved by translation of the patient bed through the homogeneous region of the gradients during image acquisition. In contrast, in whole-body mouse imaging, the entire mouse can be accommodated in a single RF coil with no need for subject or table movement. Particularly with MMMRI, where the homogeneous region of the gradient set is large relative to the size of a mouse, little modification is necessary to the gated-imaging protocol described in the above section. Whole-body mouse imaging has important applications in biomedical research for screening in cancer studies, chemical mutagenesis studies, and fat distribution or other whole-body characterizations. We have recently acquired retrospectively gated MMMRI fast spin-echo images of three whole mice at 200 μm isotropic resolution in 2 h.

FIXED AND *EX VIVO* IMAGING WITH MMMRI

Fixed-mouse imaging

In addition to supplying *in vivo* assessments of mouse phenotype, MRI can be used for three-dimensional specimen imaging in biomedical research (63,64). High-resolution, isotropic images can be acquired in specimens owing to the absence of physiological motion and the potential for long scan duration. In addition, MR measurement of tissue properties difficult to achieve in the limited scan time available *in vivo* can be achieved *ex vivo* with much finer detail. Notably, this includes measurement of fiber orientation with diffusion tensor imaging (65–69). These long *ex vivo* specimen scans can be conveniently run in ''overnight'' scan sessions with no impact on scanner resources during daytime hours. Furthermore, MRI is non-destructive so that it does not preclude later examination by traditional histological methods (70).

In addition to increased scan duration, two additional means of improving MRI efficiency are available for *ex vivo* scans. First of all, specimens can be prepared for imaging with high concentrations of contrast agents in order to considerably shorten longitudinal relaxation times. This permits shorter sequence repetition times and hence more rapid data acquisition. Secondly, excised specimens can be placed in dedicated small-sample solenoid coils, entailing a substantial increase in SNR. Even with these improvements, however, biological studies requiring many images still necessitate efficient use of scan time and hence the throughput benefits of MMMRI remain beneficial. A brief description of these methods is provided below in the context of multiple sample imaging. A more exhaustive treatment of *ex vivo* imaging is provided elsewhere in this issue.

Specimen preparation

The chief advantage of MRI is that three-dimensional imaging can be achieved while tissue remains in its natural conformation. Imaging measurements should reflect as faithfully as possible the *in vivo* status. This must be kept in mind when preparing specimens for MRI. Preparation protocols should be designed to preserve the original tissue status to the greatest extent possible. In this aim, ''minimally invasive'' fixation procedures have been described. For whole-body fixation, cannulation of peripheral blood vessels (71) or ultrasound-guided catheterization of the left ventricle (72) provides excellent means of delivering fixation agents while preserving body integrity. A high concentration of contrast agent, typically a gadolinium chelate, is included in the perfusate to shorten longitudinal relaxation time and/or improve image contrast. With these protocols, high-quality,

DOI: 10.1002/nbm

high-resolution images of the entire mouse have been acquired.

If only a single organ or portion of the body is of interest, then it is beneficial to excise the specimen and image *ex vivo*. Even in this case, however, it is desirable to maintain the original tissue conformation as much as possible. A fixation procedure that leaves supporting bone structure intact is one means of limiting potential distortions. The brain, for instance, can be left in the skull during fixation and imaging. Interestingly, the free distribution of contrast agent may be hampered by this protocol, particularly in the brain, where circulating contrast agent does not cross the blood–brain barrier during the standard fixation procedure. As a result, longitudinal relaxation times remain long, and scan efficiency is adversely affected. Therefore, it is advantageous to soak the brain and skull in a solution with gadolinium contrast agent for several days in order to permit diffusive distribution of the contrast agent (69). At the end of this period, fixed-brain images can be acquired both *in situ* and with a high concentration of contrast agent. Similar procedural modifications may be applicable for other organs or specimens.

MMMRI solenoid coil array

Although imaging of whole-body specimens can be performed in the volume coils previously discussed, dedicated small-sample solenoid coils provide improved SNR efficiency for small specimens. In their simplest form, solenoids with equal rung spacing can be wound on a threaded screw. Improved B_1 field homogeneity is achieved by reducing rung spacing towards each end of the coil (73). As image quality in MMMRI must be uniform in all coils, the reproducibility of coil fabrication is critical for MMMRI applications. To ensure reproducible production of solenoid coils with non-uniformly spaced rungs, we designed a custom manufacturing device depicted in Fig. 5a. The coils produced by this device accommodate 13-mm sample tubes, which can

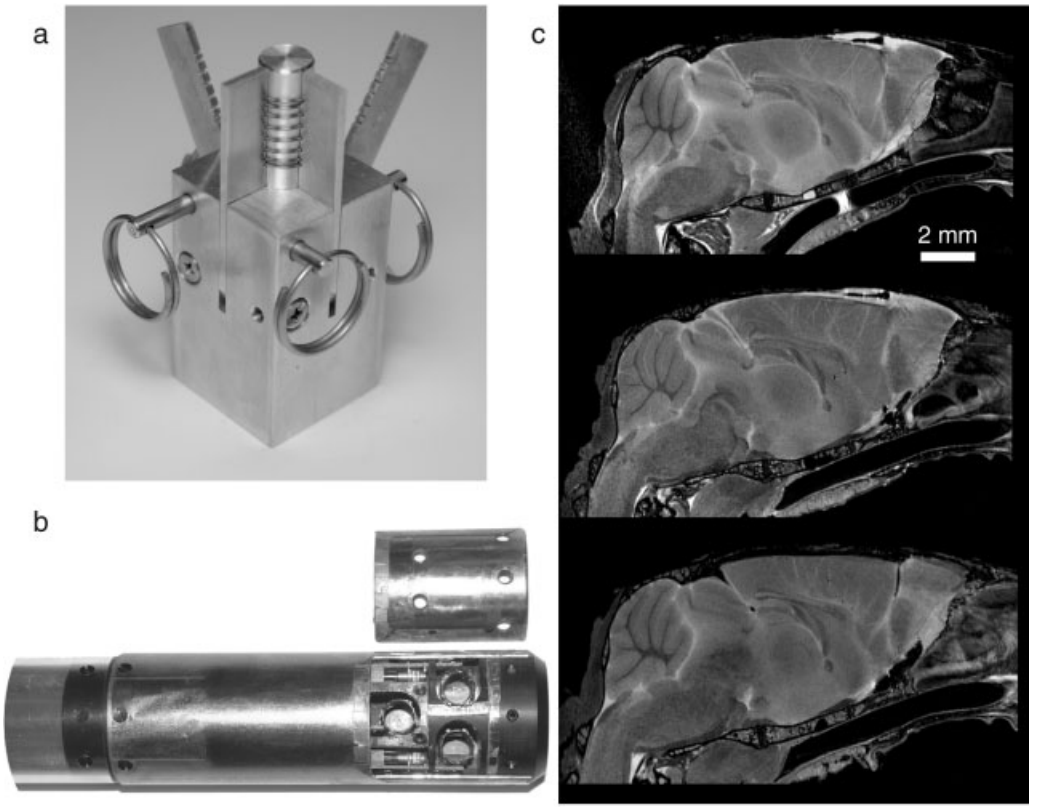

Figure 5. Multiple-specimen imaging. Reliable production of solenoid coils with variable rung spacing is facilitated by a dedicated device with notched teeth prescribing the rung spacing as shown in (a). Rung spacing is decreased at each end of the coil to improve B_1 field homogeneity. Three of these coils fit in a specimen array (b), which fits within a 60-mm bore. RF shielding between and around the coils permits tight coil spacing with minimal cross-talk between channels. In (c), three sample brain images (acquired *in situ* with the skull intact) are shown. Images were acquired with a fast-spin echo sequence with parameters including: $TR = 325$ ms, $TE = 8$ ms, 6 echoes, $TE_{eff} = 32$ ms, 6 echoes, NEX = 4, FOV 14 mm × 14 mm × 25 mm, acquisition matrix of 432 × 432 × 780, and 32-μm isotropic resolution. Total imaging time was 11 h 34 min.

DOI: 10.1002/nbm

hold specimens as large as the mouse brain and skull (after removal of extracranial tissue).

As in MMMRI with birdcage coils, RF shielding is required to isolate neighboring solenoid coils. The same style of cylindrical copper shielding on MMMRI birdcage coils can be used for solenoids as well. However, the axis of the shield would have to be perpendicular to the coil axis, an arrangement that is not ideal for packing or loading of the coils. An alternative configuration is therefore desirable. For this reason, we have constructed a small 60-mm outer-diameter, three-coil specimen imaging array (74) as depicted in Fig. 5b for use in an insert gradient. In this case, RF shielding is provided with 40-μm copper sheets glued around the interior of the outer wall and along planes between the solenoid coils, completely encasing each coil. This multiple-solenoid array is used routinely at our laboratory for simultaneous acquisition of three 32-μm isotropic images in overnight scan sessions (11.5 h scan duration). Examples of three brain images are provided in Fig. 5c.

MMMRI data analysis

If the imaging acquisition is appropriately streamlined, then the most time consuming part of mouse imaging studies becomes data analysis. With images from many different mice in any given study, a focus on efficient, grouped analysis methods is necessary. A series of mouse images in one or more experimental groups must be considered together and compared against a group of control images. To avoid bias and missed findings, the analysis procedure should be systematic and thorough. In this regard, mouse imaging has more in common with several large-scale, disease-specific human studies (10–17,75) than with clinical radiology. In these cases, hundreds of patients were imaged and their data pooled for computational analyses. The sheer number of images in these studies prevents meaningful analysis by manual observation. Similar analyses are appropriate for data processing in mouse studies. Fortunately, the genetic, and corresponding phenotypic, homogeneity in the mouse greatly reduces the number of subjects required in most mouse studies. Nevertheless, any portion of the analysis that can be performed computationally is likely to speed up results and reduce laborious manual efforts.

It is consequently advantageous to automate much of the analysis procedure. Although each type of imaging study requires some level of customization, there are several steps that are common to most studies. With three-dimensional datasets from many mice, the first step is to identify corresponding regions of anatomy between images. On a voxel-by-voxel basis, this can be achieved by automated image registration. Several packages (76–78) designed originally for analyses of human images are available for this purpose and apply equally well to mouse images. It is convenient also to define a representative and unbiased ''average'' image for each group of mice. An initial average image can be estimated by intensity averaging of images linearly aligned in an unbiased fashion. The estimate is refined with iterative nonlinear registration at progressively finer scales as described by Kovacevic *et al*. (79). The resultant average image can then be used as a basis for visual comparison with other groups of mice, while computational comparisons continue to include all images in the dataset. Group comparisons may be based on size, shape or volume of anatomy, mean voxel intensity in regions of interest, or other extractable image parameters. Significance can be established statistically by comparing the differences between groups to the variability within groups.

Anatomy, although one of the more intuitive bases of comparison, can be challenging to implement quantitatively. Deformation fields produced by the registration of individual images to the average image encode morphological differences and biological variability. For volumetric comparison of individual structures, these deformation fields may be used to transform a single segmentation (of the average image) to all individuals in the study. The resulting volumes of segmented structures can be compared across individuals. Alternatively, quantitative comparison can be made directly from the deformation fields themselves. Differences in the average deformation field between groups represent shape changes and can be quantified statistically by a variety of methods, such as the Hotelling's T_2 field (80), which conveniently accommodates the vector nature of the deformation fields. Differences in size can be calculated with the determinant of the Jacobian matrix, which provides a measure of local changes in volume. As this is a univariate measure, statistical significance can again be assessed with a variety of methods, including Student's t test. The collective use of these methods has recently been reported by our group as an efficient means of automated image comparison for routine neuroanatomical phenotyping studies (81). The process is illustrated schematically in Fig. 6.

This sort of an analysis has been used by our laboratory for the neuroanatomical characterization of normal and mutant mice. Interestingly, a study of the neuroanatomical variation within a single mouse strain shows remarkably low levels of variability (79), but significant differences can be detected between mouse strains (82). Mice with mutations have also been compared. A mutant model of oculodentodigital dysplasia, for example, shows an altered brain shape, apparently accommodating a change in skull shape (81,83). Multiple mouse image analysis also contributed to describing the phenotype of cerebellar-deficient folia mice by detection of significant size changes in the cerebellum, inferior colliculus, ventricles and olfactory bulb (84). Several additional examples will be published shortly.

DOI: 10.1002/nbm

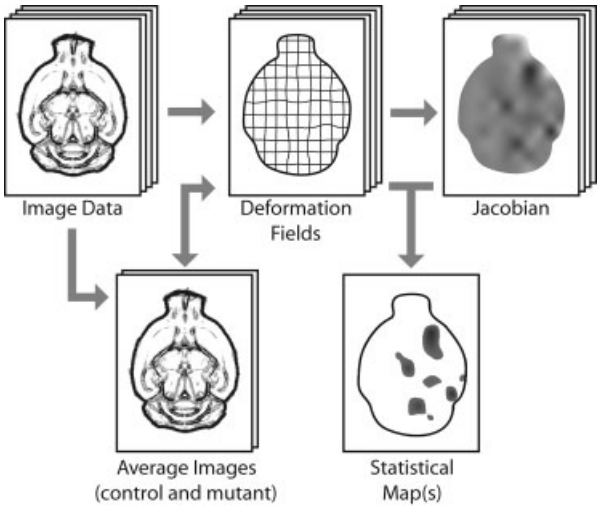

Figure 6. Multiple image dataset analysis flow chart. Images are processed by image registration to create an unbiased average of both the control and mutant groups. Iterative nonlinear registration refines the average and yields deformation fields describing the differences between each individual and the average. For the evaluation of mutant anatomy, these deformation fields can be compared directly to assess shape changes or used to calculate Jacobian fields to assess size changes. Statistical maps can be generated from both of these fields to highlight the regions of most significant change accounting for population variability. Thresholds of statistical maps can be set by various methods parametric or nonparametric methods.

It is illustrative to consider one mutant mouse study in more detail. We present, as an example, the ''bobbing head curly tail'' mutant mouse. This mutant mouse was recently generated by chemical mutagenesis and has a phenotype closely resembling the ''loop-tail'' (*Vangl2*) mutant (85). To assess possible neuroanatomical phenotypes, a set of six heterozygous mutant mice were imaged *in vivo*. Image data from four wild-type littermate mice were also acquired. To increase the size of the control group, these images were supplemented with 16 additional wild-type mice from other litters to yield a control group of 20 mouse images. Figure 7 shows the average control and average mutant images generated from this dataset and the corresponding analysis results. Inspection of the mutant images suggested hydrocephalus in the third and lateral ventricles (as indicated by green and red arrows respectively). The calculation of the average Jacobian confirmed local volume increases in these regions (Fig. 7g). Volume increases in the third ventricle were statistically the most significant changes. The lateral ventricles, on the other hand, showed a high degree of variability in the mutant group as indicated in Fig. 7h. This variability was significantly larger than the control group. Total ventricle volume, as determined by segmentation, indicated the same trends, with an increase in both ventricle volume and variability in the mouse mutant population (Fig. 7i). Phenotypes of this kind, which show either variable penetrance or severity, complicate detection of significant differences between experimental groups and motivate the use of larger numbers of mice. High-throughput methods such as MMMRI are consequently essential to these studies.

DISCUSSION

The data described in this paper were collected using a dedicated 7 T MMMRI scanner. Although this arrangement permits a high level of customization, MMMRI need not require a dedicated system. Indeed, the original demonstration of MMMRI was on a modified clinical scanner (18). As resources permit, clinical MRI scanners could be easily converted for mouse imaging in off-hours. A compact ''multiple-mouse insert'' could be constructed on a patient bed and moved in and out of the MR room as required. This insert could include a high-performance insert gradient and a resident multiple mouse coil array with an anesthetic system. On the basis of the time typically required to switch between a full-bore gradient and an insert gradient, switching between human and mouse imaging could be achieved routinely in 15–20 min. With widespread interest in dedicated insert gradients for head and extremity imaging, insert gradients of this kind are already available. Alternatively, high-performance clinical gradients could be used with no switching. Likewise, with sensitivity-encoded imaging standard on modern clinical systems, multiple transmitters and receivers along with associated image reconstruction software are also widespread. The only custom hardware required for conversion of a clinical scanner to a mouse imaging system is thus the mouse RF coils and an anesthetic system. Where a clinical scanner is available, this represents a much lower start-up cost and initial period of development than would be required for a dedicated system.

At present, MMMRI has been implemented with volume transmit/receive coils, for the whole mouse, the mouse head, the mouse thorax or individual specimens. Although this represents a good starting point, much is to be gained from more sophisticated coil arrangements. Clinical imaging, as an example, has come to depend on a number of application-specific coils and coil arrays for most examinations. These dedicated configurations provide tremendous improvements in spatial and/or temporal resolution. The same trend in coil technology is inevitable in mouse imaging. The increased sensitivity of receive-only surface coils and coil arrays, with an independent volume transmit coil, will provide enhancements to image quality. These improvements are equally available to MMMRI and single-mouse MRI. The extension to multiple mice is an interesting case. One could imagine multiple mice, with multiple coils for each mouse requiring 100 or more receive channels. Given the number of channels available on many modern commercial

DOI: 10.1002/nbm

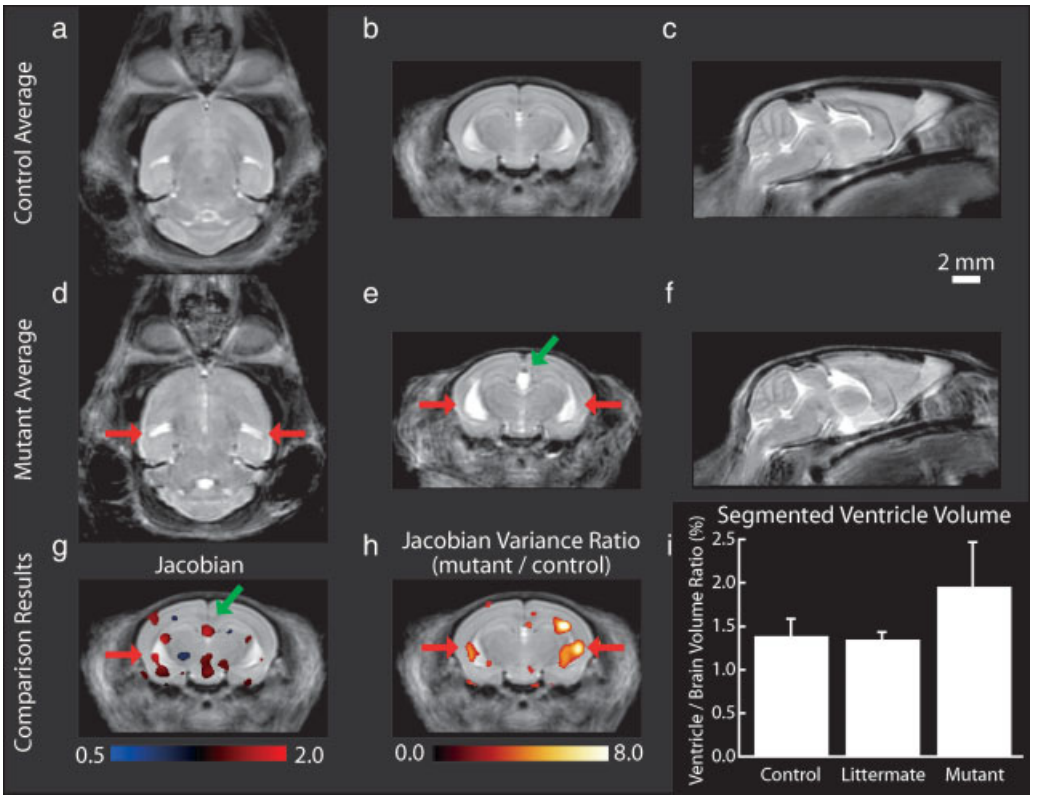

Figure 7. Neuroimaging results in a mutant mouse generated by chemical mutagenesis. Images of six heterozygous ''bobbing head curly tail'' mice were acquired with an *in vivo* fast-spin echo sequence ($TR = 900$ ms, $TE = 12$ ms, $TE_{eff} = 36$ ms, $40 \times 24 \times 24$ mm FOV, and $384 \times 208 \times 208$ matrix, total scan duration 2 h 45 min). These mice were compared with a pool of 20 control images (consisting of littermate controls of several different mutants in the same mutagenesis program). Horizontal, axial and sagittal images are shown for both the control average (a–c) and mutant average (d–f) images. Red arrows and green arrows indicate hydrocephalus at the lateral and third ventricles. Image analysis revealed significantly elevated Jacobian values at the third ventricle (g). The Jacobian map is shown with a threshold set at a 5% false discovery rate. Elevated Jacobian values at the lateral ventricles trended toward significance; however, high variability in the degree of hydrocephalus at the lateral ventricles was also evident. This variability is demonstrated in (h), where the Jacobian variance of mutant data is shown as a ratio with the control. The variance ratio overlay is shown in regions where it exceeds 2.8 (corresponding to $p < 0.05$). Manual segmentation of the average images with transformation to each of the individuals allowed ventricle volume to be assessed directly and confirmed the trends indicated by the computational analysis. In (i), ventricle volume in mutant mice was significantly increased compared with the 20 control mouse dataset ($p = 0.0003$) the subset of four ''bobbing head curly tail'' littermate controls ($p = 0.05$). Error bars indicate standard deviation of ventricle volume.

MR systems, such multiple-coil arrays for multiple-mouse applications are becoming feasible. However, in practice, the need to manage the cabling for such a system efficiently and to flexibly change the number of coils or number of mice suggest that such parallel MMMRI configurations will require another generation of receive hardware based on USB (86) or wireless coil technology (87) with a scalable modular design.

Of particular interest to several types of study, including cardiac imaging studies and *in vivo* anatomical studies where motion artifacts must be eliminated, is gradient performance. There is a clear trade-off between bore size and gradient strength. For the purpose of achieving high spatial and temporal resolution, the gradients should be specified to image as fast as possible. This means using a high slew rate and strong gradient fields. On the other hand, to accommodate large biological studies, the gradient bore should be large to accommodate as many RF coils as possible. Unfortunately, as the bore gets larger, the gradient strength is inherently weaker. The MMMRI system used in the experiments for this paper accommodates as many as 19 mice, but is ill-suited for rapid imaging. A better compromise between these two demands can be reached. For instance, a gradient coil with 200 mm inner bore diameter, 450 mT/m amplitude and 1800 mT/m/ms would fit 8–10 of the 50-mm outer-diameter birdcage coils from our current system yet still permit rapid cardiac imaging

DOI: 10.1002/nbm

applications. Advanced MMMRI configurations of this kind can be expected in the future.

The cardiac gating methodology described here used physiological monitoring from external devices. This is a straightforward way of utilizing data from the physiological monitoring already necessary during the imaging experiment. However, even in human imaging, gating based on ECG and other signals can be problematic, particularly in cases of cardiac or respiratory disease. This continues to motivate development of MRI techniques in which gating can be achieved directly from MR data with the aim of more accurately detecting physiological motions that affect MR images. These techniques are also applicable in mouse imaging. The acquisition of additional signals such as navigator echoes must be limited, however, because mouse MRI is generally signal-starved. Improved coil technology may help in this regard. Alternatively, recent techniques for self-gated imaging have been reported that derive motion information direct from imaging data (88–90). This may prove to be a preferable alternative, particularly for MMMRI.

The efficient comparison of images in large biological studies will be critical to MMMRI in particular but also to mouse MRI as a whole. Although the basic features of the multiple-mouse analysis presented here are likely to remain a common theme, many improvements to automated and semi-automated data analyses will be tremendously beneficial. Needed are whole-body image-registration techniques that incorporate realistic joint articulation, independent organ motion based on interdigitated segmentation and registration, and automated shape and texture analysis of organs. Additional analysis techniques that would be beneficial include: statistical models for controlling error when making millions of comparisons; automated registration in the presence of large intensity changes; and techniques taking into account a time dimension for dynamic contrast enhancement and motion characterization. Fortunately, these areas of mouse MRI analysis have much in common with image processing within and outside the MR community. The growing importance of image processing for both clinical and research applications ensures that this will remain an active area of development. Thus, progress in other areas will also contribute to mouse MRI applications.

CONCLUSIONS

With the ability to modify genes in the mouse, scientists have gained tremendous control of experimental conditions and an improved ability to decipher the role of genes in human disease and development. Tools for assessment of physiology, behavior, anatomy and other parameters as a function of genetic alterations are fundamental to the design and outcomes of these studies. The need to observe anatomical and functional changes *in vivo* in soft tissues throughout the body motivates growth in mouse imaging. The mouse MRI technology reviewed in this paper enables larger, more powerful biological studies and thus permits a more prominent role for mouse MRI in biomedical research. In this capacity, mouse MRI stands to make major contributions to our understanding of mouse genetics and disease pathology, which in turn will provide new avenues for the understanding and treatment of human disease.

Acknowledgements

We gratefully acknowledge funding support from the Canada Foundation for Innovation/Ontario Innovation Trust, Ontario Research and Development Challenge Fund, and the National Institutes of Health. M.H. is a recipient of a Canada Research Chair in Imaging. We are indebted to Janet Rossant, S. Lee Adamson, Ann M. Flenniken and Lucy R. Osborne of the Centre for Modeling Human Disease for supplying the mutant described in this paper.

REFERENCES

1. International Human Genome Sequencing Consortium. Finishing the euchromatic sequence of the human genome. *Nature* 2004; **431**: 931–945.
2. International HapMap Consortium. The international HapMap project. *Nature* 2003; **426**: 789–796.
3. Cargill M, Altshuler D, Ireland J, Sklar P, Ardlie K, Patil N, Lane CR, Lim EP, Kalyanaraman N, Nemesh J, Ziaugra L, Friedland L, Rolfe A, Warrington J, Lipshutz R, Daley GQ, Lander ES. Characterization of single-nucleotide polymorphisms in coding regions of human genes. *Nat. Genet.* 1999; **22**: 231–238.
4. International SNP Map Working Group. A map of human genome sequence variation containing 1.42 million single nucleotide polymorphisms. *Nature* 2001; **409**: 928–933.
5. Hrabe de Angelis MH, Flaswinkel H, Fuchs H, Rathkolb B, Soewarto D, Marschall S, Heffner S, Pargent W, Wuensch K, Jung M, Reis A, Richter T, Alessandrini F, Jakob T, Fuchs E, Kolb H, Kremmer E, Schaeble K, Rollinski B, Roscher A, Peters C, Meitinger T, Strom T, Steckler T, Holsboer F, Klopstock T, Gekeler F, Schindewolf C, Jung T, Avraham K, Behrendt H, Ring J, Zimmer A, Schughart K, Pfeffer K, Wolf E, Balling R. Genome-wide, large-scale production of mutant mice by ENU mutagenesis. *Nat. Genet.* 2000; **25**: 444–447.
6. Nolan PM, Peters J, Strivens M, Rogers D, Hagan J, Spurr N, Gray IC, Vizor L, Brooker D, Whitehill E, Washbourne R, Hough T, Greenaway S, Hewitt M, Liu X, McCormack S, Pickford K, Selley R, Wells C, Tymowska-Lalanne Z, Roby P, Glenister P, Thornton C, Thaung C, Stevenson JA, Arkell R, Mburu P, Hardisty R, Kiernan A, Erven A, Steel KP, Voegeling S, Guenet JL, Nickols C, Sadri R, Nasse M, Isaacs A, Davies K, Browne M, Fisher EM, Martin J, Rastan S, Brown SD, Hunter J. A systematic, genome-wide, phenotype-driven mutagenesis programme for gene function studies in the mouse. *Nat. Genet.* 2000; **25**: 440–443.
7. The chipping forecast. *Nat. Genet.* **21**(1s): 1999.
8. The chipping forecast II. *Nat. Genet.* **32**(4s): 2002.
9. McConville P, Moody JB, Moffat BA. High-throughput magnetic resonance imaging in mice for phenotyping and therapeutic evaluation. *Curr. Opin. ion. Chem. Biol.* 2005; **9**: 413–420.
10. Gaser C, Volz HP, Kiebel S, Riehemann S, Sauer H. Detecting structural changes in whole brain based on nonlinear deformations-application to schizophrenia research. *Neuroimage* 1999; **10**: 107–113.

11. Jack CR Jr, Petersen RC, O'Brien PC, Tangalos EG. MR-based hippocampal volumetry in the diagnosis of Alzheimer's disease. *Neurology* 1992; **42**: 183–188.
12. Jack CR Jr, Petersen RC, Xu YC, Waring SC, O'Brien PC, Tangalos EG, Smith GE, Ivnik RJ, Kokmen E. Medial temporal atrophy on MRI in normal aging and very mild Alzheimer's disease. *Neurology* 1997; **49**: 786–794.
13. Aylward EH, Li Q, Stine OC, Ranen N, Sherr M, Barta PE, Bylsma FW, Pearlson GD, Ross CA. Longitudinal change in basal ganglia volume in patients with Huntington's disease. *Neurology* 1997; **48**: 394–399.
14. Aylward EH, Anderson NB, Bylsma FW, Wagster MV, Barta PE, Sherr M, Feeney J, Davis A, Rosenblatt A, Pearlson GD, Ross CA. Frontal lobe volume in patients with Huntington's disease. *Neurology* 1998; **50**: 252–258.
15. Giedd JN, Castellanos FX, Casey BJ, Kozuch P, King AC, Hamburger SD, Rapoport JL. Quantitative morphology of the corpus-callosum in attention-deficit hyperactivity disorder. *Am. J. Psychiatry* 1994; **151**: 665–669.
16. Hynd GW, Semrudclikeman M, Lorys AR, Novey ES, Eliopulos D. Brain morphology in developmental dyslexia and attention-deficit disorder hyperactivity. *Arch. Neurol.* 1990; **47**: 919–926.
17. Hynd GW, Semrudclikeman M, Lorys AR, Novey ES, Eliopulos D, Lyytinen H. Corpus-callosum morphology in attention deficit-hyperactivity disorder: morphometric analysis of MRI. *J. Learn. Disabil.* 1991; **24**: 141–146.
18. Bock NA, Konyer NB, Henkelman RM, Multiple-mouse MRI. *Magn Reson. Med* 2003; **49**: 158–167.
19. Xu S, Gade TP, Matei C, Zakian K, Alfieri AA, Hu X, Holland EC, Soghomonian S, Tjuvajev J, Ballon D, Koutcher JA. *In vivo* multiple-mouse imaging at 1.5 T. *Magn Reson. Med* 2003; **49**: 551–557.
20. Schneider JE, Bose J, Bamforth SD, Gruber AD, Broadbent C, Clarke K, Neubauer S, Lengeling A, Bhattacharya S. Identification of cardiac malformations in mice lacking Ptdsr using a novel high-throughput magnetic resonance imaging technique. *BMC. Dev. Biol* 2004; **4**: 16.
21. Matsuda Y, Utsuzawa S, Kurimoto T, Haishi T, Yamazaki Y, Kose K, Anno I, Marutani M. Super-parallel MR microscope. *Magn. Reson. Med* 2003; **50**: 183–189.
22. Nieman BJ, Bock NA, Bishop J, Chen XJ, Sled JG, Rossant J, Henkelman RM. Magnetic resonance imaging for detection and analysis of mouse phenotypes. *NMR Biomed.* 2005; **18**: 447–468.
23. Langlois S, Desvignes M, Constans JM, Revenu M. MRI geometric distortion: a simple approach to correcting the effects of non-linear gradient fields. *J. Magn. Reson. Imaging* 1999; **9**: 821–831.
24. Bock NA, Zadeh G, Davidson LM, Qian B, Sled JG, Guha A, Henkelman RM. High-resolution longitudinal screening with magnetic resonance imaging in a murine brain cancer model. *Neoplasia* 2003; **5**: 546–554.
25. Sodickson DK, Hardy CJ, Zhu YD, Giaquinto RO, Gross P, Kenwood G, Niendorf T, Lejay H, McKenzie CA, Ohliger MA, Grant AK, Rofsky NM. Rapid volumetric MRI using parallel imaging with order-of-magnitude accelerations and a 32-element RF coil array: feasibility and implications. *Academic Radiology* 2005; **12**: 626–635.
26. Bock NA, Nieman BJ, Bishop JB, Henkelman RM. *In vivo* multiple-mouse MRI at 7 Tesla. *Magn. Reson. Med.* 2005; **54**: 1311–1316.
27. Wong WH. Millipede coils. Varian, Inc., assignee. Patent US 6,285,189 B1. 9 Apr. 2001.
28. Dazai J, Bock NA, Nieman BJ, Davidson LM, Henkelman RM, Chen XJ. Multiple mouse biological loading and monitoring system for MRI. *Magn. Reson. Med.* 2004; **52**: 709–715.
29. Harsan LA, Poulet P, Guignard B, Steibel J, Parizel N, de Sousa PL, Boehm N, Grucker D, Ghandour MS. Brain dysmyelination and recovery assessment by noninvasive *in vivo* diffusion tensor magnetic resonance imaging. *J. Neurosci. Res.* 2006; **83**: 392–402.
30. Kim JH, Budde MD, Liang HF, Klein RS, Russell JH, Cross AH, Song SK. Detecting axon damage in spinal cord from a mouse model of multiple sclerosis. *Neurobiology of Disease* 2006; **21**: 626–632.
31. Xue R, Sawada M, Goto S, Hurn PD, Traystman RJ, van Zijl PC, Mori S. Rapid three-dimensional diffusion MRI facilitates the study of acute stroke in mice. *Magn. Reson. Med.* 2001; **46**: 183–188.
32. Mueggler T, Meyer-Luehmann M, Rausch M, Staufenbiel M, Jucker M, Rudin M. Restricted diffusion in the brain of transgenic mice with cerebral amyloidosis. *Eur. J Neurosci.* 2004; **20**: 811–817.
33. Hiba B, Richard N, Janier M, Croisille P. Cardiac and, respiratory double self-gated cine MRI in the mouse at 7 T. *Magn. Reson. Med.* 2006; **55**: 506–513.
34. Nahrendorf M, Hiller KH, Hu K, Ertl G, Haase A, Bauer WR. Cardiac magnetic resonance imaging in small animal models of human heart failure. *Medical Image Analysis* 2003; **7**: 369–375.
35. Ross AJ, Yang Z, Berr SS, Gilson WD, Petersen WC, Oshinski JN, French BA. Serial MRI evaluation of cardiac structure and function in mice after reperfused myocardial infarction. *Magn. Reson. Med.* 2002; **47**: 1158–1168.
36. Wiesmann F, Ruff J, Engelhardt S, Hein L, Dienesch C, Leupold A, Illinger R, Frydrychowicz A, Hiller KH, Rommel E, Haase A, Lohse MJ, Neubauer S. Dobutamine-stress magnetic resonance microimaging in mice: acute changes of cardiac geometry and function in normal and failing murine hearts. *Circ. Res.* 2001; **88**: 563–569.
37. Zhou R, Pickup S, Glickson JD, Scott CH, Ferrari VA. Assessment of global and regional myocardial function in the mouse using cine and tagged MRI. *Magn. Reson. Med.* 2003; **49**: 760–764.
38. Gilson WD, Yang Z, French BA, Epstein FH. Complementary displacement-encoded MRI for contrast-enhanced infarct detection and quantification of myocardial function in mice. *Magn. Reson. Med.* 2004; **51**: 744–752.
39. Natt O, Watanabe T, Boretius S, Frahm J, Michaelis T. Magnetization transfer MRI of mouse brain reveals areas of high neural density. *Magn. Reson. Imaging* 2003; **21**: 1113–1120.
40. Stanisz GJ, Odrobina EE, Pun J, Escaravage M, Graham SJ, Bronskill MJ, Henkelman RM. T-1, T-2 relaxation and magnetization transfer in tissue at 3T. *Magn. Reson. Med.* 2005; **54**: 507–512.
41. Lascola CD, Song AW, Haystead TA, Warner DS, Verleysen K, Freed TA, Provenzale JM. Changes in magnetization transfer MRI correlate with spreading depression-induced astroglial reactivity and increased protein expression in mice. *AJR Am. J. Roentgenol.* 2004; **183**: 1791–1797.
42. Guilfoyle DN, Hrabe J. Interleaved snapshot echo planar imaging of mouse brain at 7.0T. *NMR Biomed.* 2006; **19**: 108–115.
43. Nair G, Duong TQ. Echo-planar BOLD fMRI of mice on a narrow-bore 9.4 T magnet. *Magn. Reson. Med.* 2004; **52**: 430–434.
44. Ahrens ET, Dubowitz DJ. Peripheral somatosensory fMRI in mouse at 11.7 T. *NMR Biomed.* 2001; **14**: 318–324.
45. Wu EX, Tang H, Asai T, Yan SD. Regional cerebral blood volume reduction in transgenic mutant APP (V717F, K670N/M671L) mice. *Neurosci. Lett.* 2004; **365**: 223–227.
46. Mueggler T, Sturchler-Pierrat C, Baumann D, Rausch M, Staufenbiel M, Rudin M. Compromised hemodynamic response in amyloid precursor protein transgenic mice. *J. Neurosci.* 2002; **22**: 7218–7224.
47. Beckmann N, Schuler A, Mueggler T, Meyer EP, Wiederhold KH, Staufenbiel M, Krucker T. Age-dependent cerebrovascular abnormalities and blood flow disturbances in APP23 mice modeling Alzheimer's disease. *Journal of Neuroscience* 2003; **23**: 8453–8459.
48. Aime S, Cabella C, Colombatto S, Geninatti CS, Gianolio E, Maggioni F. Insights into the use of paramagnetic Gd(III) complexes in MR-molecular imaging investigations. *J. Magn. Reson. Imaging* 2002; **16**: 394–406.
49. Artemov D. Molecular magnetic resonance imaging with targeted contrast agents. *J. Cell. Biochem.* 2003; **90**: 518–524.
50. Wadghiri YZ, Sigurdsson EM, Sadowski M, Elliott JI, Li YS, Scholtzova H, Tang CY, Aguinaldo G, Pappolla M, Duff K, Wisniewski T, Turnbull DH. Detection of Alzheimer's amyloid in Transgenic mice using magnetic resonance microimaging. *Magn. Reson. Med.* 2003; **50**: 293–302.
51. Poduslo JF, Wengenack TM, Curran GL, Wisniewski T, Sigurdsson EM, Macura SI, Borowski BJ, Jack CR. Molecular targeting of Alzheimer's amyloid plaques for contrast-enhanced magnetic resonance imaging. *Neurobiology of Disease* 2002; **11**: 315–329.

DOI: 10.1002/nbm

52. Yu X, Wadghiri YZ, Sanes DH, Turnbull DH. *In vivo* auditory brain mapping in mice with Mn-enhanced MRI. *Nature Neuroscience* 2005; **8**: 961–968.
53. Koretsky AP, Silva AC. Manganese-enhanced magnetic resonance imaging (MEMRI). *NMR Biomed.* 2004; **17**: 527–531.
54. Aoki I, Naruse S, Tanaka C. Manganese-enhanced magnetic resonance imaging (MEMRI) of brain activity and applications to early detection of brain ischemia. *NMR Biomed.* 2004; **17**: 569–580.
55. Pautler RG, Mongeau R, Jacobs RE. *In vivo* trans-synaptic tract tracing from the murine striatum and amygdala utilizing manganese enhanced MRI (MEMRI). *Magn Reson Med* 2003; **50**: 33–39.
56. Pautler RG, Silva AC, Koretsky AP. *In vivo* neuronal tract tracing using manganese-enhanced magnetic resonance imaging. *Magn. Reson. Med.* 1998; **40**: 740–748.
57. Genove G, DeMarco U, Xu HY, Goins WF, Ahrens ET. A new transgene reporter for *in vivo* magnetic resonance imaging. *Nat. Med.* 2005; **11**: 450–454.
58. Deans AE, Yu X, Wadghiri YZ, Duan XC, Turnbull DH. 7T-MRI of transferrin receptor and ferritin gene expression in a mouse neural stem cell line. At the *International Society for Magnetic Resonance in Medicine 13th Scientific Meeting*. May 2005; Miami Beach, FL, USA.
59. Ruff J, Wiesmann F, Hiller KH, Voll S, von Kienlin M, Bauer WR, Rommel E, Neubauer S, Haase A. Magnetic resonance microimaging for noninvasive quantification of myocardial function and mass in the mouse. *Magn. Reson. Med.* 1998; **40**: 43–48.
60. Lenz GW, Haacke EM, White RD. Retrospective cardiac gating: a review of technical aspects and future directions. *Magn. Reson. Imaging* 1989; **7**: 445–455.
61. Bohning DE, Carter B, Liu SS, Pohost GM. PC-based system for retrospective cardiac and respiratory gating of NMR data. *Magn Reson. Med.* 1990; **16**: 303–316.
62. Bishop J, Feintuch A, Bock NA, Nieman B, Dazai J, Davidson L, Henkelman RM. Retrospective gating for mouse cardiac MRI. *Magn. Reson. Med.* 2006; **55**: 472–477.
63. Dhenain M, Ruffins SW, Jacobs RE. Three-dimensional digital mouse atlas using high-resolution MRI. *Dev. Biol.* 2001; **232**: 458–470.
64. Johnson GA, Cofer GP, Fubara B, Gewalt SL, Hedlund LW, Maronpot RR. Magnetic resonance histology for morphologic phenotyping. *J. Magn. Reson. Imaging* 2002; **16**: 423–429.
65. Guilfoyle DN, Helpern JA, Lim KO. Diffusion tensor imaging in fixed brain tissue at 7.0 T. *NMR Biomed* 2003; **16**: 77–81.
66. Sun SW, Neil JJ, Song SK. Relative indices of water diffusion anisotropy are equivalent in live and formalin-fixed mouse brains. *Magn. Reson. Med.* 2003; **50**: 743–748.
67. Zhang J, Miller MI, Yarowsky P, van Zijl P, Mori S. Mapping postnatal mouse brain development with diffusion tensor microimaging. *Neuroimage* 2005; **26**: 1042–1051.
68. Jiang Y, Pandya K, Smithies O, Hsu EW. Three-dimensional diffusion tensor microscopy of fixed mouse hearts. *Magn. Reson. Med.* 2004; **52**: 453–460.
69. Tyszka JM, Readhead C, Bearer EL, Pautler RG, Jacobs RE. Statistical diffusion tensor histology reveals regional dysmyelination effects in the shiverer mouse mutant. *Neuroimage* 2006; **29**: 1058–1065.
70. Spencer RG, Fishbein KW, Cheng AW, Mattson MP. Compatibility of Gd-DTPA perfusion and histologic studies of the brain. *Magn. Reson. Imaging* 2006; **24**: 27–31.
71. Johnson GA, Cofer GP, Gewalt SL, Hedlund LW. Morphologic phenotyping with MR microscopy: the visible mouse. *Radiology* 2002; **222**: 789–793.
72. Zhou YQ, Davidson L, Henkelman RM, Nieman BJ, Foster FS, Yu LX, Chen XJ. Ultrasound-guided left-ventricular catheterization: a novel method of whole mouse perfusion for microimaging. *Lab. Invest.* 2004; **84**: 385–389.
73. Idziak S, Haeberlen U. Design and construction of a high homogeneity Rf coil for solid-state multiple-pulse NMR. *J. Magn. Reson.* 1982; **50**: 281–288.
74. Li Y, Wolters AM, Malawey PV, Sweedler JV, Webb AG. Multiple solenoidal microcoil probes for high-sensitivity, high-throughput nuclear magnetic resonance spectroscopy. *Anal. Chem.* 1999; **71**: 4815–4820.
75. Jernigan TL, Salmon DP, Butters N, Hesselink JR. Cerebral Structure on Mri .2. Specific changes in Alzheimers and Huntingtons diseases. *Biol. Psychiatry* 1991; **29**: 68–81.
76. Collins DL, Evans AC. Animal: Validation and applications of nonlinear registration-based segmentation. *International Journal of Pattern Recognition and Artificial Intelligence* 1997; **11**: 1271–1294.
77. Woods RP, Grafton ST, Holmes CJ, Cherry SR, Mazziotta JC. Automated image registration. I. General methods and intrasubject, intramodality validation. *J. Comput. Assist. Tomogr.* 1998; **22**: 139–152.
78. Woods RP, Grafton ST, Watson JD, Sicotte NL, Mazziotta JC. Automated image registration. II. Intersubject validation of linear and nonlinear models. *J. Comput. Assist. Tomogr.* 1998; **22**: 153–165.
79. Kovacevic N, Henderson JT, Chan E, Lifshitz N, Bishop J, Evans AC, Henkelman RM, Chen XJ. A three-dimensional MRI atlas of the mouse brain with estimates of the average and variability. *Cerebral Cortex* 2005; **15**: 639–645.
80. Cao J, Worsley KJ. The detection of local shape changes via the geometry of Hotelling's T-2 fields. *Ann. Stat.* 1999; **27**: 925–942.
81. Nieman BJ, Flenniken AM, Adamson SL, Henkelman RM, Sled JG. Anatomical phenotyping in the brain and skull of a mutant mouse by magnetic resonance imaging and computed tomography. *Physiol Genomics* 2006; **24**: 154–162.
82. Chen XJ, Kovacevic N, Lobaugh NJ, Sled JG, Henkelman RM, Henderson JT. Neuroanatomical differences between mouse strains as shown by high-resolution 3D MRI. *Neuroimage* 2006; **29**: 99–105.
83. Flenniken AM, Osborne LR, Anderson N, Ciliberti N, Fleming C, Gittens JE, Gong XQ, Kelsey LB, Lounsbury C, Moreno L, Nieman BJ, Peterson K, Qu D, Roscoe W, Shao Q, Tong D, Veitch GI, Voronina I, Vukobradovic I, Wood GA, Zhu Y, Zirngibl RA, Aubin JE, Bai D, Bruneau BG, Grynpas M, Henderson JE, Henkelman RM, McKerlie C, Sled JG, Stanford WL, Laird DW, Kidder GM, Adamson SL, Rossant J. A Gja1 missense mutation in a mouse model of oculodentodigital dysplasia. *Development* 2005; **132**: 4375–4386.
84. Bock NA, Kovacevic N, Lipina TV, Roder JC, Ackerman SL, Henkelman RM. *In vivo* magnetic resonance imaging and semiautomated image analysis extend the brain phenotype for cdf/cdf mice. *J. Neurosci.* 2006; **26**: 4455–4459.
85. Kibar Z, Vogan KJ, Groulx N, Justice MJ, Underhill DA, Gros P. Ltap a mammalian homolog of *Drosophila* Strabismus/Van Gogh, is altered in the mouse neural tube mutant Loop-tail. *Nat. Genet.* 2001; **28**: 251–255.
86. Stang P, Conolly S, Pauly J, Scott G. A USB approach to scalable design of MRI systems. At the *International Society for Magnetic Resonance in Medicine 13th Scientific Meeting and Exhibition.* May 2005; Miami Beach, FL, USA.
87. Scott GC, Yu K. Wireless transponders for RF coils: systems issues. At the *International Society for Magnetic Resonance in Medicine 13th Scientific Meeting and Exhibition.* May 2005; Miami Beach, FL, USA.
88. Crowe ME, Larson AC, Zhang Q, Carr J, White RD, Li D, Simonetti OP. Automated rectilinear self-gated cardiac cine imaging. *Magn. Reson. Med.* 2004; **52**: 782–788.
89. Larson AC, White RD, Laub G, McVeigh ER, Li D, Simonetti OP. Self-gated cardiac cine MRI. *Magn. Reson. Med.* 2004; **51**: 93–102.
90. Brau AC, Brittain JH. Self-navigation motion detection technique generalized for arbitrary pulse sequences. At the *Thirteenth Scientific Meeting and Exhibition.* International Society for Magnetic Resonance in Medicine. May 2005; Miami Beach, Florida.

DOI: 10.1002/nbm